Plasmonic Vesicles of Amphiphilic Gold Nanocrystals: Self-Assembly and External-Stimuli-Triggered Destruction

Jibin Song,[†,§] Lin Cheng,[†,§] Aiping Liu,[†] Jun Yin,[†] Min Kuang,[‡] and Hongwei Duan*,[†]

[†]School of Chemical and Biomedical Engineering, Nanyang Technological University, 70 Nanyang Drive, Singapore 637457
[‡]Ocean Nanotech, 2143 Worth Lane, Springdale, Arkansas 72764, United States

S *Supporting Information*

ABSTRACT: We have developed a new class of plasmonic vesicular nanostructures assembled from amphiphilic gold nanocrystals with mixed polymer brush coatings. One major finding is that the integration of gold nanocrystals (nanoparticles and nanorods) with two types of chemically distinct polymer grafts, which are analogous to block copolymers as a whole, creates a new type of hybrid building block inheriting the amphiphilicity-driven self-assembly of block copolymers to form vesicular structures and the plasmonic properties of the nanocrystals. In contrast to other vesicular structures, the disruption of the plasmonic vesicles can be triggered by stimulus mechanisms inherent to either the polymer or the nanocrystal. Recent advances in nanocrystal synthesis and controlled surface-initiated polymerization have opened a wealth of possibilities for expanding this concept to other types of nanocrystals and integrating different types of nanocrystals into multifunctional vesicles. The development of multifunctional vesicles containing stimuli-responsive polymers could enable their broader applications in biosensing, multimodality imaging, and theragnostic nanomedicine.

Figure 1. Schematic illustration of self-assembly of amphiphilic nanocrystals with mixed polymer brushes into vesicular structures.

Self-assembled vesicular structures with a water-filled compartment enclosed by a thin shell are of considerable interest in many fields ranging from materials sciences to biophysics and nanomedicine.[1] Varieties of building blocks for constructing vesicles for the encapsulation and delivery of active ingredients such as drug molecules and optical probes have been actively explored.[1,2] Natural and synthetic amphiphiles can assemble into liposomes with a bilayer structure mimicking the cell membrane through self-aggregation of their hydrophobic tails in an aqueous medium.[1b,c,3] Similarly, amphiphilicity-driven self-assembly of block copolymers gives rise to polymersomes with tailored mechanical and structural properties.[4,5] Advances in chemistry leading toward well-defined polymeric amphiphiles with diverse functionalities have enabled the development of polymersomes whose permeabilities are responsive to external stimuli such as pH, light, and enzymatic degradation.[6,7] Recently, the growing interest in functional vesicles has stimulated research activities utilizing as building blocks metal and semiconductor nanocrystals with unique optical, electronic, and magnetic properties.[8−11] Nanocrystals have been incorporated into liposomes[8] and polymersomes[9] through noncovalent interactions. Alternatively, colloidosomes, which are large microcapsules composed of a monolayer of densely packed nanocrystals, have been obtained through the interfacial
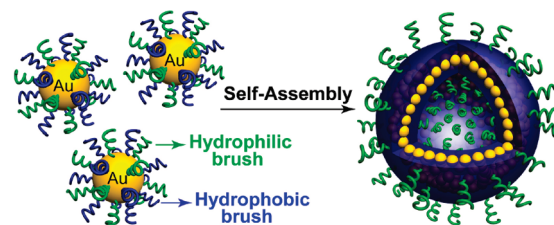
self-assembly of nanocrystals driven by the decrease in total free energy.[10] Recent work by several groups has also shown that nanocrystals with single-component polymer brush coatings can assemble into vesicles by taking advantage of the different hydrophobicities of the nanocrystals and polymer brushes.[11]

Here we report a new class of plasmonic vesicular nanostructures assembled from amphiphilic nanocrystals with mixed polymer brush coatings, as illustrated in Figure 1. Organization of nanocrystals with polymer brush coatings into well-defined assemblies is the subject of intense research.[11,12] Our results have shown that the integration of gold nanocrystals (nanoparticles and nanorods) with two types of chemically distinct polymer grafts, which are analogous to block copolymers as a whole, creates a new type of hybrid building block inheriting the amphiphilicity-driven self-assembly of block copolymers to form vesicular structures and the plasmonic properties of the nanocrystals. In the vesicles, the nanocrystals impart their intriguing properties to the assembly, and in addition, the strong interparticle plasmonic coupling leads to collective properties different from those in discrete units. More interestingly, the covalently anchored "smart" polymer grafts provide a means of modulating the interparticle coupling through their stimuli-responsive conformational changes, making the plasmonic vesicles potential candidates for integrated delivery and sensing applications. This is clearly not available for nanocrystal-loaded polymersomes (liposomes) and colloidosomes because of the absence of responsive mechanisms and the noncovalent linking between the vesicle shell and nanocrystals. The vesicles have sizes on the nanometer scale (~200 nm), which is similar to polymersomes but much smaller than colloidosomes (mostly tens to hundreds of micrometers in size), although nanocrystals form closely attached monolayers in the shells of both assemblies. Another interesting finding is that destruction of the
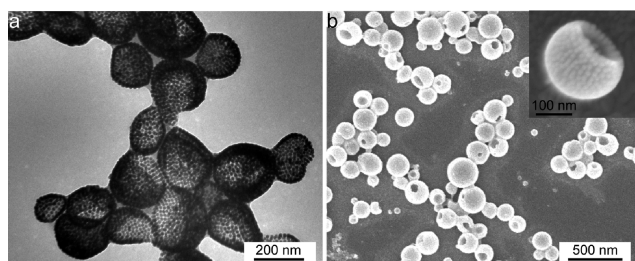
Figure 2. TEM (a) and SEM (b) images of the plasmonic vesicles assembled from 14 nm gold nanocrystals with mixed poly(ethylene glycol) and poly(methyl methacrylate) brushes.

Figure 3. (a) UV–vis spectra of the amphiphilic nanocrystals in chloroform and the vesicles in aqueous media: Au@PEG/PMMA (black solid line), vesicles of Au@PEG/PMMA (black dashed line), Au@PEG/PMMAVP containing 25% 4VP in the hydrophobic brush (red solid line), vesicles of Au@PEG/PMMAVP at pH 7.0 (red dashed line), and the disassembled vesicles of Au@PEG/PMMAVP at pH 5.0 (red dot line). (b, c) Dark-field microscope images of the vesicles of Au@PEG/PMMAVP at (b) pH 7.0 and (c) pH 5.0.

plasmonic vesicles can be triggered not only by external stimuli specific to the amphiphilic polymer grafts but also by the photo-thermal conversion property of gold nanorods in the near-IR (NIR) spectral window (650– 900 nm).

Amphiphilic nanocrystals with mixed polymer brushes were synthesized through a two-step approach consisting of sequentially conducted "grafting to" and "grafting from" reactions, as we reported recently [see the Supporting Information (SI)].[13] The first step was a ligand exchange reaction in which hydrophilic poly(ethylene glycol) (PEG) and the atom-transfer radical polymerization (ATRP) initiator 2,2′-dithiobis[1-(2-bromo-2-methylpropionyloxy)]ethane (DTBE) were simultaneously attached to gold nanocrystals through covalent Au–S bonds. In the second step, the purified nanocrystals were used as macro-initiators for surface-initiated ATRP of hydrophobic or stimuli-response monomers. This strategy offers the possibility of integrating chemically distinct polymer grafts on nanocrystals with well-controlled physicochemical properties and the flexibility to tune the structural parameters (ratio, molecular weight, and graft density) of the mixed polymer brushes.[14] In this study, the plasmonic vesicles were formed using the film rehydration method, which is commonly used for the preparation of polymersomes (see the SI). We first examined the self-assembly of 14 nm gold nano-particles with PEG and hydrophobic poly(methyl methacrylate) (PMMA) grafts (Au@PEG/PMMA). The nanoparticles carry 88 PEG (M_n = 5 kDa) and 176 PMMA (M_n = 22 kDa) grafts on average, as calculated on the basis of the molar ratio (PEG: PMMA = 1:2) of the two grafts deduced from ^{1}H NMR and molecular weight information and the weight fraction (20%) of organic polymer brushes measured by thermogravimetric analysis (see the SI).[13] Transmission electron microscopy (TEM) observation (Figure 2a) of the resultant vesicles showed a characteristic image of hollow structures with a clear contrast between the interior and the shell. The polymer part is not visible in the TEM image because of its poor contrast. The shell thickness was measured to be equal to the diameter of the gold nanoparticle, suggesting that the shell of the vesicle is composed of a monolayer array of nanocrystals. Scanning electron microscopy (SEM) (Figure 2b) further confirmed that the vesicles have a hollow cavity enclosed by a thin shell. At higher magnification, closely attached individual nanoparticles on the shell are clearly visible. The vesicles retained their spherical morphology without collapse after they were dried under vacuum, indicative of their excellent mechanical stability. In the shell of the vesicle, it is expected that nanocrystals are embedded in the collapsed hydrophobic PMMA grafts, and the hydrophilic PEG chains reorganize to face the aqueous environment on either side of the shell, as displayed in Figure 1.
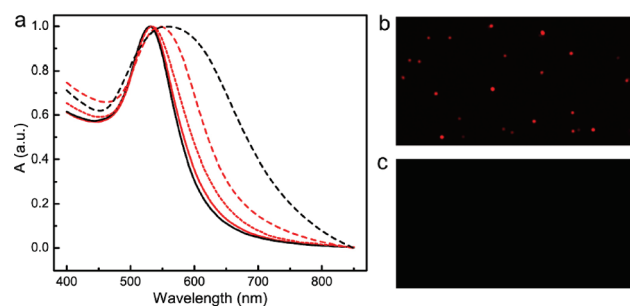
The surface plasmon resonance (SPR) of gold nanoparticles is extremely sensitive to changes in the local environment surrounding the particles and to the interparticle distances.[15] In UV–vis spectra (Figure 3a), the SPR band of the plasmonic vesicles shows a 30 nm red shift relative to the SPR band of the discrete nanoparticles in chloroform (530 nm) that is due to the strong interparticle plasmonic coupling in the shell. Recent developments in surface-initiated ATRP have made it possible to graft well-defined polymers of functional monomers onto nanocrystals, providing access to new building blocks with stimuli-sensitive surface coatings.[16] In a model system, we introduced 25% 4-vinylpyridine (4VP, pK_a = 5.4)[17] in the hydrophobic PMMA grafts (Figure S1 in the SI), creating pH-responsive plasmonic vesicles using the pH-sensitive nanocrystal (Au@PEG/PMMAVP). Figure 3a shows that the SPR peak (546 nm) of the Au@PEG/PMMAVP vesicles was also red-shifted at pH 7.0, as observed for the vesicles without the 4VP moiety, but to a lesser extent. This should arise from the electrostatic repulsion induced by the partially protonated pyridine groups at pH 7.0, which increases the interparticle distances of the gold nanoparticles and reduces the plasmonic coupling as a result. We also found that the degree of plasmonic coupling in the vesicles can be tuned by changing the amount of 4VP. For example, the vesicle containing 10% 4VP had an SPR peak centered at 550 nm (Figure S2), which lies between those of the vesicle with 100% PMMA and the one with 25% 4VP. It should be noted that the interparticle distances shown in the TEM images of the two vesicles (Figure 2a and Figure S3) are not significantly different because TEM images show the dry state under high vacuum. When the pH was tuned from 7.0 to 5.0, the SPR peak of the vesicle experienced a sudden blue shift to 536 nm (Figure 3a and Figure S4), and TEM observation revealed that vesicles dissociated into single nanoparticles and small clusters of nanoparticles. This was also manifested by the results of dynamic light scattering measurements, which showed that vesicles with diameters of ~260 nm disintegrated into smaller particles with hydrodynamic sizes of ~30 nm (Figure S5). This pH-triggered disruption of the vesicle can potentially be used for intracellular delivery of therapeutic agents by taking advantage of the acidic environment in the endocytic pathway.[18] Plasmonic nanoparticles scatter light very strongly at the SPR wavelengths.[15b] We found that scattering from individual vesicles can be easily detected using a dark-field
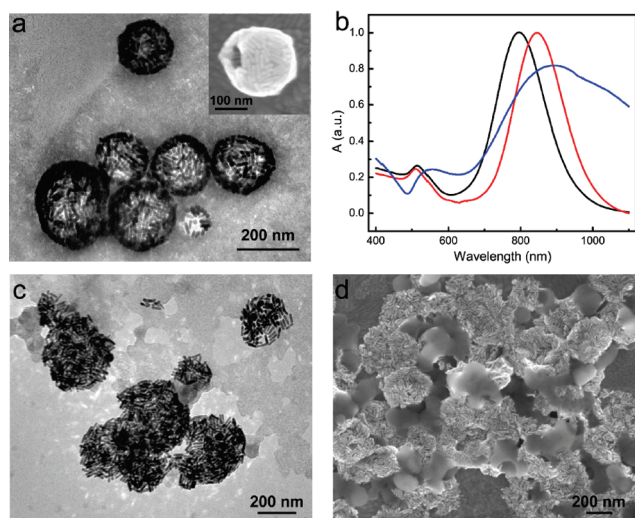
Figure 4. Self-assembly and NIR-irradiation-induced disruption of AuNR@PEG/PMMA vesicles. (a) TEM and (inset) SEM images of the vesicle. (b) UV−vis spectra of as-prepared gold nanorods coated with cetyltrimethylammonium bromide (black line), AuNR@PEG/PMMA in chloroform (red line), and the nanorod vesicles (blue line). (c) TEM and (d) SEM images of a vesicle after 2 min of irradiation with a 785 nm laser.

microscope (Figure 3b) and that the signal completely disappeared after the pH decreased from 7.0 to 5.0 (Figure 3c). The scattering cross sections of single nanoparticles are highly dependent on their sizes,[19] and the 14 nm gold nanoparticles used here exhibited negligible light scattering. Obviously, the plasmonic coupling in vesicles leads to a greatly enhanced scattering cross section, which decreases dramatically after the vesicles disintegrate into single nanoparticles at pH 5.0. This ON/OFF switch of light scattering between vesicles and single nanoparticles can be used to monitor the disintegration of the vesicles using a dark-field microscope, which would allow the release of payloads encapsulated in the vesicles to be traced in real time.

Plasmonic nanostructures can rapidly convert the light absorbed at the SPR wavelengths into thermal energy to heat up the surrounding medium.[15b] This photothermal conversion property has attracted tremendous attention in the development of plasmonic nanomaterials for photothermal therapy[20] and remotely controlled drug delivery.[21] Particularly for in vivo applications, nanostructures with SPR bands in the NIR spectral window are highly desirable because of the smaller extent of attenuation of light by blood and soft tissue in this spectral range.[22] Gold nanorods have emerged as promising candidates for this purpose because their longitudinal plasmon resonance can easily be tuned into the NIR region by variation of their aspect ratio.[20a,d] Here we utilized gold nanorods ($\sim$13 nm $\times$ 51 nm) with mixed PEG and PMMA brushes (AuNR@PEG/PMMA) to prepare plasmonic vesicles (see the SI). Figure 4a shows that vesicles with diameters of $\sim$200 nm were successfully obtained. Interestingly, all of the anisotropic nanorods were aligned parallel to the vesicle surface, as shown in the SEM image (Figure 4a inset). The nanorod length is 51 nm, and the contour length of a fully stretched PEG chain (M_n = 5 kDa) is $\sim$50 nm. If the nanorods had been oriented perpendicular to the surface, a large portion of the hydrophilic PEG grafts would have

been trapped inside the hydrophobic core of the shell. Therefore, the orientation along the surface to form a dense monolayer is thermodynamically more favorable for the anisotropic nanorods. UV−vis spectrometry (Figure 4b) showed that in the vesicle, both the transverse and longitudinal plasmon resonances of the gold nanorods were red-shifted and became broader because of the strong plasmonic coupling of the nanorods in close proximity. Next, we tested the light-induced deconstruction of the vesicles by irradiating a drop of vesicle dispersion on substrates with a 785 nm diode laser at 2 W/cm^2. TEM and SEM observations (Figure 4c,d) revealed that the vesicles lost their spherical morphology after 2 min of irradiation and were disrupted into flattened aggregates, confirming that the localized heating generated by the assembled gold nanorods was sufficient to induce collapse of the PMMA shell. Notably, the vesicles are thermally stable enough for applications under physiological conditions, since heating at 65 °C for 30 min did not lead to evident changes in the hydrodynamic size distribution of the vesicles (Figure S6). Obviously, in contrast to many other plasmonic structures, the photothermal treatment and the chemotherapeutic agents hosted in the large cavity could generate a synergistic effect when the nanorod vesicles are used for therapeutic applications.

In summary, we have presented a new type of plasmonic vesicular structure based on amphiphilic nanocrystals with mixed polymer brush coatings as building blocks. In three model vesicles of plasmonic gold nanostructures, we have demonstrated that the new building blocks consisting of a "hard" nanocrystal core and "soft" polymeric grafts provide unprecedented opportunities for flexible tuning of the collective optical properties of the vesicles and triggering of vesicle disruption by stimulus mechanisms inherent to either the polymer or the nanocrystal. Recent developments in nanocrystal synthesis and controlled surface-initiated polymerization have opened a wealth of possibilities for expanding this concept to other types of nanocrystals and integrating different types of nanocrystals into multifunctional vesicles. We envision that the development of multifunctional vesicles containing stimuli-responsive polymers could enable their broader applications in biosensing, multimodality imaging, and theragnostic nanomedicine.

■ ASSOCIATED CONTENT

ⓢ Supporting Information. Experimental details, supporting figures, and complete ref 3a. This material is available free of charge via the Internet at http://pubs.acs.org.

■ AUTHOR INFORMATION

Corresponding Author
hduan@ntu.edu.sg

Author Contributions
§These authors contributed equally.

■ ACKNOWLEDGMENT

■ REFERENCES

(1) (a) Discher, D. E.; Eisenberg, A. *Science* **2002**, *297*, 967–973. (b) Szoka, F. C.; Guo, X. *Acc. Chem. Res.* **2003**, *36*, 335–341. (c) Sawant, R. R.; Torchilin, V. P. *Soft Matter* **2010**, *6*, 4026–4044.

(2) (a) Böker, A.; He, J.; Emrick, T.; Russell, T. P. *Soft Matter* **2007**, *3*, 1231–1248. (b) Wang, D. Y.; Duan, H. W.; Möhwald, H. *Soft Matter* **2005**, *1*, 412–416.

(3) (a) Percec, V.; et al. *Science* **2010**, *328*, 1009–1014. (b) Zhang, X.; Rehm, S.; Safont-Sempere, M. M.; Würthner, F. *Nat. Chem.* **2009**, *1*, 623–629.

(4) (a) Discher, B. M.; Won, Y. Y.; Ege, D. S.; Lee, J. C. M.; Bates, F. S.; Discher, D. E.; Hammer, D. A. *Science* **1999**, *284*, 1143–1146. (b) Huang, H. Y.; Remsen, E. E.; Kowalewski, T.; Wooley, K. L. *J. Am. Chem. Soc.* **1999**, *121*, 3805–3806.

(5) (a) Duan, H. W.; Chen, D. Y.; Jiang, M.; Gan, W. J.; Li, S. J.; Wang, M.; Gong, J. *J. Am. Chem. Soc.* **2001**, *123*, 12097–12098. (b) Kuang, M.; Duan, H. W.; Wang, J.; Jiang, M. *J. Phys. Chem. B* **2004**, *108*, 16023–16029.

(6) van Dongen, S. F. M.; de Hoog, H. P. M.; Peters, R. J. R. W.; Nallani, M.; Nolte, R. J. M.; van Hest, J. C. M. *Chem. Rev.* **2009**, *109*, 6212–6274.

(7) (a) Mynar, J. L.; Goodwin, A. P.; Cohen, J. A.; Ma, Y. Z.; Fleming, G. R.; Fréchet, J. M. J. *Chem. Commun.* **2007**, 2081–2082. (b) Napoli, A.; Valentini, M.; Tirelli, N.; Müller, M.; Hubbell, J. A. *Nat. Mater.* **2004**, *3*, 183–189. (c) Katz, J. S.; Zhong, S.; Ricart, B. G.; Pochan, D. J.; Hammer, D. A.; Burdick, J. A. *J. Am. Chem. Soc.* **2010**, *132*, 3654–3655.

(8) (a) Al-Jamal, W. T.; Al-Jamal, K. T.; Tian, B. W.; Lacerda, L.; Bomans, P. H.; Frederik, P. M.; Kostarelos, K. *ACS Nano* **2008**, *2*, 408–418. (b) Rasch, M. R.; Rossinyol, E.; Hueso, J. L.; Goodfellow, B. W.; Arbiol, J.; Korgel, B. A. *Nano Lett.* **2010**, *10*, 3733–3739.

(9) (a) Chen, R.; Pearce, D. J. G.; Fortuna, S.; Cheung, D. L.; Bon, S. A. F. *J. Am. Chem. Soc.* **2011**, *133*, 2151–2153. (b) Sanson, C.; Diou, O.; Thévenot, J.; Ibarboure, E.; Soum, A.; Brûlet, A.; Miraux, S.; Thiaudière, E.; Tan, S.; Brisson, A.; Dupuis, V.; Sandre, O.; Lecommandoux, S. *ACS Nano* **2011**, *5*, 1122–1140.

(10) (a) Lin, Y.; Skaff, H.; Emrick, T.; Dinsmore, A. D.; Russell, T. P. *Science* **2003**, *299*, 226–229. (b) Duan, H. W.; Wang, D. Y.; Sobal, N. S.; Giersig, M.; Kurth, D. G.; Mohwald, H. *Nano Lett.* **2005**, *5*, 949–952. (c) Arumugam, P.; Patra, D.; Samanta, B.; Agasti, S. S.; Subramani, C.; Rotello, V. M. *J. Am. Chem. Soc.* **2008**, *130*, 10046–10047. (d) Yang, X. C.; Samanta, B.; Agasti, S. S.; Jeong, Y.; Zhu, Z. J.; Rana, S.; Miranda, O. R.; Rotello, V. M. *Angew. Chem., Int. Ed.* **2011**, *50*, 477–481. (e) Fortuna, S.; Colard, C. A. L.; Troisi, A.; Bon, S. A. F. *Langmuir* **2009**, *25*, 12399–12403.

(11) (a) Nie, Z. H.; Fava, D.; Kumacheva, E.; Zou, S.; Walker, G. C.; Rubinstein, M. *Nat. Mater.* **2007**, *6*, 609–614. (b) Nikolic, M. S.; Olsson, C.; Salcher, A.; Kornowski, A.; Rank, A.; Schubert, R.; Frömsdorf, A.; Weller, H.; Förster, S. *Angew. Chem., Int. Ed.* **2009**, *48*, 2752–2754. (c) Whitelam, S.; Bon, S. A. F. *J. Chem. Phys.* **2010**, *132*, No. 074901.

(12) Zubarev, E. R.; Xu, J.; Sayyad, A.; Gibson, J. D. *J. Am. Chem. Soc.* **2006**, *128*, 15098–15099.

(13) Cheng, L.; Liu, A. P.; Peng, S.; Duan, H. W. *ACS Nano* **2010**, *4*, 6098–6104.

(14) (a) Shan, J.; Nuopponen, M.; Jiang, H.; Viitala, T.; Kauppinen, E.; Kontturi, K.; Tenhu, H. *Macromolecules* **2005**, *38*, 2918–2926. (b) Zubarev, E. R.; Xu, J.; Sayyad, A.; Gibson, J. D. *J. Am. Chem. Soc.* **2006**, *128*, 4958–4959.

(15) (a) Rosi, N. L.; Mirkin, C. A. *Chem. Rev.* **2005**, *105*, 1547–1562. (b) Jain, P. K.; Huang, X. H.; El-Sayed, I. H.; El-Sayed, M. A. *Acc. Chem. Res.* **2008**, *41*, 1578–1586. (c) Tao, A. R.; Habas, S.; Yang, P. *Small* **2008**, *4*, 310–325.

(16) (a) Matyjaszewski, K.; Xia, J. *Chem. Rev.* **2001**, *101*, 2921–2990. (b) Edmondson, S.; Osborne, V. L.; Huck, W. T. S. *Chem. Soc. Rev.* **2004**, *33*, 14–22.

(17) Kuang, M.; Wang, D. Y.; Bao, H. B.; Gao, M. Y.; Möhwald, H.; Jiang, M. *Adv. Mater.* **2005**, *17*, 267–270.

(18) Duan, H. W.; Nie, S. M. *J. Am. Chem. Soc.* **2007**, *129*, 3333–3338.

(19) Jain, P. K.; Lee, K. S.; El-Sayed, I. H.; El-Sayed, M. A. *J. Phys. Chem. B* **2006**, *110*, 7238–7248.

(20) (a) Huang, X. H.; El-Sayed, I. H.; Qian, W.; El-Sayed, M. A. *J. Am. Chem. Soc.* **2006**, *128*, 2115–2120. (b) Chen, J. Y.; Wang, D. L.; Xi, J. F.; Au, L.; Siekkinen, A.; Warsen, A.; Li, Z. Y.; Zhang, H.; Xia, Y. N.; Li, X. D. *Nano Lett.* **2007**, *7*, 1318–1322. (c) You, J.; Zhang, G. D.; Li, C. *ACS Nano* **2010**, *4*, 1033–1041. (d) von Maltzahn, G.; Park, J. H.; Agrawal, A.; Bandaru, N. K.; Das, S. K.; Sailor, M. J.; Bhatia, S. N. *Cancer Res.* **2009**, *69*, 3892–3900.

(21) (a) Hu, K. W.; Liu, T. M.; Chung, K. Y.; Huang, K. S.; Hsieh, C. T.; Sun, C. K.; Yeh, C. S. *J. Am. Chem. Soc.* **2009**, *131*, 14186–14187. (b) Jin, Y. D.; Gao, X. H. *J. Am. Chem. Soc.* **2009**, *131*, 17774–17776. (c) Kuo, T. R.; Hovhannisyan, V. A.; Chao, Y. C.; Chao, S. L.; Chiang, S. J.; Lin, S. J.; Dong, C. Y.; Chen, C. C. *J. Am. Chem. Soc.* **2010**, *132*, 14163–14171. (d) Huschka, R.; Neumann, O.; Barhoumi, A.; Halas, N. J. *Nano Lett.* **2010**, *10*, 4117–4122.

(22) Frangioni, J. V. *Curr. Opin. Chem. Biol.* **2003**, *7*, 626–634.